Earth Surf. Dynam. Discuss., doi:10.5194/esurf-2016-57, 2016
Manuscript under review for journal Earth Surf. Dynam.
Published: 1 December 2016

Earth Surface Dynamics Discussions

Constraining Quaternary erosion of the Campine Plateau (NE Belgium) using Bayesian inversion of an in-situ produced ^{10}Be concentration depth profile

Koen Beerten[1], Eric Laloy[1], Veerle Vanacker[2], Bart Rogiers[1], Laurent Wouters[3]

[1]Institute Environment-Health-Safety, Belgian Nuclear Research Centre (SCK•CEN), Mol, 2400, Belgium
[2]Georges Lemaitre Centre for Earth and Climate Research, Earth and Life Institute, Université catholique de Louvain, Louvain-la-Neuve, 1348, Belgium
[3]Long-term RD&D department, Belgian National Agency for Radioactive Waste and enriched Fissile Material (ONDRAF/NIRAS), Brussels, 1210, Belgium

Correspondence to: Koen Beerten (kbeerten@sckcen.be)

Abstract. The rate at which low-lying sandy areas in temperate regions, such as the Campine area (NE Belgium), have been eroding during the Quaternary is a matter of debate. Current knowledge on the average pace of landscape evolution in the Campine area is largely based on geological inferences and modern analogies. We applied Bayesian inversion to an in-situ produced ^{10}Be concentration depth profile in fluvial sand, sampled on top of the Campine Plateau, and inferred the average long-term erosion rate together with three other parameters, i.e., the surface exposure age, inherited ^{10}Be concentration and sediment bulk density. The inferred erosion rate of 44 ± 9 mm/kyr (1σ) is relatively large in comparison with landforms that erode under comparable (palaeo-)climates elsewhere in the world. We evaluate this value in the light of the erodibility of the substrate and sudden base level lowering during the Middle Pleistocene. A denser sampling scheme of a two-nuclide concentration depth profile would allow to include more parameters in the model inversion and further reduce their uncertainty.

1 Introduction

The Campine area is a sandy region which covers part of northeastern Belgium and the southern Netherlands (Fig. 1). It is part of the European sand belt and is drained by rivers that belong to the Scheldt basin. The Campine area roughly coincides with the geological Campine Basin, being the southeastern part of the North Sea Basin. From a geodynamic point of view, the Campine Basin is located in an intermediate position in between the rapidly subsiding Roer Valley Graben in the north, and the uplifting Brabant and Ardennes Massifs in the south (Fig. 2). The Campine Basin has witnessed a long Cenozoic burial history. Post-Rupelian marine and estuarine deposition during the last 30 Ma almost exclusively consists of (glauconite-rich) sand, up to 300 m thick (Vandenberghe et al., 2004). From the Early to Middle Pleistocene onwards, terrestrial conditions become dominant with deposition of a thick series of fluvial sand and gravel from the rivers Meuse and

Earth Surf. Dynam. Discuss., doi:10.5194/esurf-2016-57, 2016
Manuscript under review for journal Earth Surf. Dynam.
Published: 1 December 2016

Rhine (Figs. 2 and 3). In contrast to what the basinal setting of the Campine region would suggest, distinctive topographic features are preserved in the landscape. An illustrative example is the Campine Plateau, which shows a topographic relief of ca. 50 m relative to the surrounding areas (Fig. 3). To date, quantitative data on the amount and rate of Quaternary erosion of the Campine landscape and the Scheldt basin in general are missing. This stands in contrast to the availability of long-term erosion data from e.g. in-situ produced cosmogenic nuclides for the Meuse and Rhine basins (e.g., Schaller et al., 2001; Dehnert et al., 2011; Rixhon et al., 2011). Such data on catchment-wide erosion rates at multi-millennial timescales are crucial to determine background geological erosion rates to evaluate anthropogenic morphodynamics (Vanacker et al., 2007a), to provide calibration data for landscape evolution models (Bogaart and van Balen, 2000; Foster et al., 2015; Campforts et al., 2016), and to assess the overall stability of the landscape in the framework of long-term management of radioactive waste (Van Geet et al., 2012).

Cosmogenic radionuclides (CRN's) have proven useful to quantify geomorphological processes over timespans covering the last 1 Ma (Schaller et al., 2001). Geomorphological surfaces can be dated by measuring the concentration of in-situ produced cosmogenic nuclides (e.g., ^{10}Be and ^{26}Al) that accumulated at the Earth's surface (Hancock et al., 1999; Hein et al., 2009). As the observed cosmogenic nuclide concentration of a given outcrop is a function of its exposure age and denudation rate, stable (i.e. non-eroding) landforms provide optimal sampling locations for exposure dating (e.g., Rixhon et al., 2011). Most landforms are subject to erosion during exposure, resulting in a decrease of the cosmogenic nuclide concentrations with increasing surface denudation rate (e.g., Dehnert et al., 2011). Braucher et al. (2009) showed that the exposure age (and post-depositional denudation rate) of eroding landforms can be constrained based on a deep (> 1,5 m) depth profile of a single cosmogenic nuclide that is sampled at regular intervals.

The accumulation of in-situ produced cosmogenic nuclides in eroding surfaces is a mathematical function with two parameters that are typically unknown a priori: the exposure age, t [y], and the post-depositional denudation rate, E [cm/y]. Unknown model parameters can be estimated by inverse modeling of CRN concentration vs. depth profiles. In this procedure, one iteratively proposes new parameter values until the model fits the observed data up to a pre-specified precision. This has been done for estimating t and E by, e.g., Siame et al. (2004) and Braucher et al. (2009). Yet, model and measurement errors together with (measurement) data scarcity introduce considerable uncertainty in optimizing the model parameters. The method proposed by Braucher et al. (2009) accounts to some extent for analytical measurement errors, as it generates several CRN concentration profiles consistent with the (analytical) measurement errors, computes for each model parameter set (e.g., a *t-E* pair) within a grid search the corresponding data misfits and retains the median misfit as the performance associated with a given parameter set. This allows for deriving a robust unique solution but does not consider explicitly model parameter uncertainty and ignores model errors (that is, the model is assumed to be perfect). A more comprehensive quantification of parameter and prediction uncertainty is provided by the Bayesian framework. This approach represents parameter uncertainty by a multivariate “posterior” probability distribution, which is consistent with both prior

Earth Surf. Dynam. Discuss., doi:10.5194/esurf-2016-57, 2016
Manuscript under review for journal Earth Surf. Dynam.
Published: 1 December 2016

information and the (CRN) concentration measurements. In this work, we derive the model parameter posterior probability density function (pdf) by state-of-the-art Markov chain Monte Carlo simulation (see, e.g., Robert and Casella, 2004), accounting under certain assumptions for both measurement and model errors.

The overall objective of this study is to constrain within a Bayesian framework the rate and amount of post-depositional denudation of the headwaters of the Nete catchment. The latter is part of the larger Scheldt basin and is used herein to test and demonstrate the application of Bayesian inversion to CRN concentration vs. depth profiles. The Nete catchment is an interesting test case because the upstream areas of the catchment are located at the northwestern edge of the Campine Plateau, which is covered by coarse gravelly sand from the Early-Middle Pleistocene Rhine and thus constitutes a fluvial terrace from which the depositional age nor the exposure age of the sands is well constrained (Beerten et al., in press).

2 Geomorphological evolution of the Campine area

The post-marine hydrographical evolution of the Campine area started with the final retreat of the sea during the Neogene, as a result of systematic sea level lowering and overall uplift of the bordering areas around the southern North Sea (Miller et al. 2005; Cloething et al. 2007). During the Early Pleistocene, the Meuse followed an eastern course from Liège to the region north of Aachen where it merged with the Rhine (Fig. 2). Tectonic movements along Roer Valley Graben faults, and uplift of the northern margins of the Ardennes-Eifel massif caused the Meuse to breach through its northern interfluve and to follow a completely different course. At the same time, the Rhine shifted its course as well, flowing into the northern part of the Campine area where it merged with the Meuse (Fig. 2). Age control is limited, but this event probably took place around 1 Ma at the earliest, since the confluence area of both rivers was situated in the southeastern part of the Roer Valley Graben prior to 1 Ma, and the area that covers the Campine Plateau today was drained by local 'Belgian' rivers until that time (Westerhoff et al., 2008). Both rivers shifted their course towards a more eastern position by 0.5 Ma at the latest, given the absence of Rhine deposits younger than 0.5 Ma in the depocenter of the Roer Valley Graben (Schokker et al. 2005). The deposits that cover the Campine Plateau are often correlated with the upstream Main Terraces of the Meuse and High Terraces of the Rhine (Paulissen, 1973). Westaway (2001) provides a time window for deposition of Rhine sediments west of the Ville Ridge (High Terraces HT2 and HT3) between 0.5 Ma and 1 Ma. The Rhine sediments on top of the Campine Plateau have been attributed to the Sterksel Formation, which was deposited between ca. 0.6 Ma and 1.1 Ma according to van Balen et al. (2000), and between ca. 0.75 Ma and 1 Ma (post-Jaramillo Early-Pleistocene) according to Gullentops et al., (2001). Recently, deposits from the High Terraces of the Rhine between Bonn (Germany) and Venlo (the Netherlands) have been dated to 750 ± 250 ka and 740 ± 210 ka using in-situ produced cosmogenic radionuclides (Dehnert et al., 2011). Similarly, Meuse terrace deposits in the Liège area (Romont, Belgium) that are generally assumed to correspond with the series of Main Terrace deposits, have been dated to 725 ± 120 ka using the same technique (Rixhon et al., 2011).

Earth Surf. Dynam. Discuss., doi:10.5194/esurf-2016-57, 2016
Manuscript under review for journal Earth Surf. Dynam.
Published: 1 December 2016

During the Middle Pleistocene, the hydrography of northern Belgium drastically changed due to the 'opening' of the English Channel (Vandenberghe and De Smedt 1979; Fig. 2). Various studies (Gibbard 2007; Gupta et al. 2007; Toucanne et al. 2009) link the opening of the English Channel to the catastrophic drainage of a large proglacial lake during marine isotope stage 12 (MIS 12), approximately 450 ka ago (Elsterian). The 450 ka event triggered the formation of a buried palaeo-channel system known as the Flemish Valley, with extensions towards the south and the east (Tavernier and De Moor, 1974). The Nete catchment is generally considered as the eastern extension of the Flemish Valley.

At present, the Campine Plateau is a landform that markedly stands out with respect to its surroundings. It is a fluvial terrace covered by coarse gravelly Meuse deposits in the south(east) and sandy Rhine deposits in the north (Fig. 3). The sediments have proven to feature a periglacial palaeoenvironment and were deposited by braided rivers (Paulissen, 1973 and 1983). The Campine Plateau can be considered as a classical case of relief inversion (Fig. 4). Undoubtedly, the area west of the Campine Plateau experienced prolonged phases of erosion and denudation after the Rhine had left the region, around 0.5 Ma at the latest (Fig. 4b; Beerten et al., in press).

3 Material and methods

3.1 Cosmogenic radionuclide profiling

Cosmogenic radionuclides (CRN) allow us to quantify geomorphological processes over timespans covering the last 1 Ma. In this study, we use the concentration vs. depth profile of a single in-situ produced CRN (^{10}Be) to constrain the post-depositional denudation rate, E [cm/y] of the fluvial terrace. The accumulation of CRN, $N_{total}(z,t)$ [at/g], in an eroding surface can be described by a mathematical function composed of two terms that represent the inherited CRN concentration of the fluvial sediment, $N_{inh}(z)$, and the post-depositional production of CRN, $N_{exp}(z)$:

$$N_{total}(z,t) = N_{inh}(z) + \sum_i \frac{P_i(z)}{\lambda + \frac{\rho E}{\Lambda_i}} e^{-(\rho(z_0 - Et)/\Lambda_i} \left(1 - e^{-\left(\lambda + \frac{\rho E}{\Lambda_i}\right)t}\right) \quad (1)$$

with t [y] the exposure age, λ [1/y] the decay constant ($\lambda = \ln 2 / t_{1/2}$), z_0 the initial shielding depth ($z_0 = E \times t$), ρ [g/cm³] the density of the overlying material, Λ_i [g/cm²] the attenuation length. The production rate of CRN, $P_i(z)$ [at/g/y], is a function of the depth, z [cm], below the surface as:

$$P_i(z) = P_i(0) e^{-\frac{z\rho}{\Lambda_i}*} \quad (2)$$

The subscript 'i' indicates the different production pathways of in-situ produced ^{10}Be via spallation, muon capture and fast muons following Dunai (2010). In this study, we set the relative contribution of neutrons and muons (negative and fast) to

Earth Surf. Dynam. Discuss., doi:10.5194/esurf-2016-57, 2016
Manuscript under review for journal Earth Surf. Dynam.
Published: 1 December 2016

the total ^{10}Be production at resp. 97.85, 1.50 and 0.65%, and set the effective attenuation length at resp. 150, 1500 and 5300 g/cm² following Braucher et al. (2003). Production rates were scaled following Dunai (2001) with a sea level high latitude production rate of (4.5 ± 0.3) at/g/y. This production rate is consistent with the value that was used earlier on by Rixhon et al. (2011) for dating terraces of the Ardennian rivers. A half-life of (1.387 ± 0.012) × 10^6 y was used for ^{10}Be following Cmeleff et al. (2010). CosmoCalc add-in for Excel was used to calculate the scaling factors. Given the flat topography of the Campine Plateau, topographic shielding was negligible and therefore not corrected for (Norton and Vanacker, 2009).

3.2 Sampling and analytical methods

The depth profile was sampled in a sand pit (SRC-Sibelco NV) on the northwestern edge of the Campine Plateau (Fig. 4a and b). The altitude of the sampling spot is ca. 47 m (Tweede Algemene Waterpassing), while the crest of the plateau further east reaches an altitude of ca. 48 m. The almost 4 m thick sequence is composed of medium-grained quartz-rich fluvial sands, overlain by a thin layer (35 cm thick) of fine-grained aeolian sand (Fig. 5). Detailed grain-size characteristics of the fluvial sand are given in Fig. 6. Note that sample depth is given with reference to the top of the fluvial sands. The lowermost unit A consists of medium sand with mode and median in the range between 250-500 µm, while a significant portion of grains coarser than 500 µm is present. Unit B is finer with a median grain size of ca. 250 µm and virtually no coarse sand (i.e., > 500 µm). Unit C consists of coarse sand (median grain size more than 500 µm) with a significant amount of fine gravel fragments. The next unit (E) is the finest unit of the sequence, with mode and median below 250 µm. Sediments from unit F are generally finer than those of units A and C, but coarser than those from units B and D. Mode and median are in the range between 250-500 µm. Finally, unit G represents a thin layer of fine sand, interpreted as Late Pleistocene aeolian deposits. Based on the grain size analysis, the fluvial sequence can be divided into several fining-upward sequences, where samples MHR-II-06 and MHR-II-04 are taken in much finer sand beds compared to the other samples.

From the depth profile, ten samples were collected for CRN analysis at depths ranging from 10 to 320 cm below the fluvial-aeolian contact, from which 9 were analysed. Samples were more or less evenly spread out over the sequence, although the sampling density was higher towards the top (Table 2). Samples were taken as bulk samples of 1.5 kg, over a depth interval of 10 cm. Samples were sieved, and the 500-1000 µm grain size fraction was used for sample preparation, except for the fine-grained sand samples MHR-II-04 and MHR-II-06 where the 250-500 µm fraction had to be used.

Samples were prepared at the University of Louvain Cosmogenic Isotope Laboratory (Louvain-la-Neuve). In-situ produced ^{10}Be was extracted from purified quartz using standard separation methods described in von Blanckenburg et al. (1996) and Vanacker et al. (2007b). Two blanks were processed with the nine samples. Approximately 200 µg of ^{9}Be carrier was added to blanks and samples containing 30 to 35 g pure quartz. ^{10}Be/^{9}Be ratios were measured in BeO targets with accelerator mass spectrometry on the 0.6 MV Tandy at ETH Zurich (Kubik and Christl, 2010). The ratios were normalized to the ETH in-house secondary standard S2007N with a nominal value of ^{10}Be/^{9}Be of 28.1 × 10^{-12} (Kubik and Christl, 2010) which is in agreement with a half-life of 1.387 Myr (Chmeleff et al., 2010). Samples are corrected for the number of ^{10}Be atoms in their

Earth Surf. Dynam. Discuss., doi:10.5194/esurf-2016-57, 2016
Manuscript under review for journal Earth Surf. Dynam.
Published: 1 December 2016

160 associated blanks. The analytical uncertainties on the $^{10}Be/^{9}Be$ ratios of sample and blank are then propagated into the 1σ analytical uncertainty for nuclide concentrations.

162

3.3 Bayesian inference

164 #### 3.3.1 Inverse problem

To acknowledge that measurements and modelling errors are inevitable, the inverse problem is commonly represented by the 166 stochastic relationship given by

168 $$F(\mathbf{x}) = \mathbf{d} + \mathbf{e} \quad (3)$$

170 where F is a deterministic, error-free forward model that expresses the relation between the uncertain parameters, **x**, and the measurement data, **d**, and the noise term, **e**, lumps measurement and model errors.

172 Inversions were performed within a Bayesian framework, which treats the unknown model parameters **x** as random variables with posterior probability density function (pdf), $p(\mathbf{x}|\mathbf{d})$, given by

174

$$p(\mathbf{x}|\mathbf{d}) = \frac{p(\mathbf{d}|\mathbf{x})p(\mathbf{x})}{p(\mathbf{d})} \propto L(\mathbf{x}|\mathbf{d})p(\mathbf{x}) \quad (4)$$

176

where $p(\mathbf{x})$ denotes the prior distribution of **x** and $L(\mathbf{x}|\mathbf{d}) \equiv p(\mathbf{d}|\mathbf{x})$ signifies the likelihood function of **x**. The normalization 178 factor $p(\mathbf{d}) = \int p(\mathbf{d}|\mathbf{x})p(\mathbf{x})d\mathbf{x}$ is obtained from numerical integration over the parameter space so that $p(\mathbf{x}|\mathbf{d})$ scales to unity. The quantity $p(\mathbf{d})$ is generally difficult to estimate in practice but is not required for parameter inference. In the 180 remainder of this study, we will focus on the unnormalized posterior $p(\mathbf{x}|\mathbf{d}) \propto L(\mathbf{x}|\mathbf{d})p(\mathbf{x})$. For numerical stability, it is often preferable to work with the log-likelihood function, $\ell(\mathbf{x}|\mathbf{d})$, instead of $L(\mathbf{x}|\mathbf{d})$. If we assume the error **e** to be normally 182 distributed, uncorrelated and with unknown constant variance, σ^2, the log-likelihood function can be written as

184 $$\ell(\mathbf{x}|\mathbf{d}) = -\frac{N_d}{2}\ln(2\pi) - \frac{N_d}{2}\ln(\sigma^2) - \frac{1}{2\sigma^2}\sum_{i=1}^{N_d}[d_i - F_i(\mathbf{x})]^2 \quad (5)$$

186 where σ^2 can be fixed beforehand or sampled jointly with the other model parameters **x**. It is worth noting that by fixing σ to a known measurement error, one implicitly assumes that the model is able to describe the observed system up to the 188 observation errors. This might not be realistic in environmental modelling, where models are always fairly simplified descriptions of a more complex reality. In this work, we therefore jointly infer σ with **x.**

Earth Surf. Dynam. Discuss., doi:10.5194/esurf-2016-57, 2016
Manuscript under review for journal Earth Surf. Dynam.
Published: 1 December 2016

190 **3.3.2 Markov chain Monte Carlo sampling**

The main goal of the inference is to estimate the posterior parameter distribution of the model parameters, $p(\mathbf{x}|\mathbf{d})$. As an
192 exact analytical solution for $p(\mathbf{x}|\mathbf{d})$ is not available, we resort to Markov chain Monte Carlo (MCMC) simulation to generate samples from this distribution. The basis of this technique is a Markov chain that generates a random walk through the
194 search space and iteratively finds parameter sets with stable frequencies stemming from the posterior pdf of the model parameters (see, e.g., Robert and Casella, 2004, for a comprehensive overview of MCMC simulation). In practice, the
196 MCMC sampling efficiency strongly depends on the assumed proposal distribution used to generate transitions in the Markov chain. In this work, the state-of-the art DREAM$_{ZS}$ (ter Braak and Vrugt, 2008; Vrugt et al., 2009; Laloy and Vrugt,
198 2012) algorithm is used to generate posterior samples. A detailed description of this sampling scheme including convergence proof can be found in the literature cited and is thus not reproduced herein.
200 To constrain the post-depositional erosion rate, E, of the sampling site on the Campine Plateau, we apply Bayesian inference on the mathematical expression of the CRN concentration vs. depth profile (Eq. (1)). Details on the model parameter settings
202 are given above. The following marginal prior distributions were defined for the sampled five model parameters, based on the current geological knowledge of the region, as well as the measured ^{10}Be data (Table 1 and 2). For 3 out of 5 parameters,
204 i.e., post-depositional erosion (E), exposure age (t) and bulk density (ρ), we specified truncated Gaussian prior distributions using mid-range points of the adopted interval as means and 0.4 times the interval range as standard deviations. Our
206 justification for this choice is as follows. On the one hand, the prior distribution is sufficiently vague to avoid over-constraining the search (mid-range prior probability is only about twice that of the boundary values), and, on the other hand,
208 it discourages the search to pick up values close to the boundaries as they are considered to be (a priori) less likely. The exposure age of the terrace, t [y], was allowed to vary between 0.5 Ma and 1 Ma, based on the presumed burial age of the
210 Rhine sands covering the Campine Plateau at that location from geological evidence (see Section 2). This results in a prior mean of 0.75 Ma, and a standard deviation of 0.2 Ma. These estimates are fully consistent with CRN burial ages of 750 ±
212 250 ka and 740 ± 210 ka that were established for the High Terrace deposits from the Rhine in Germany and the Netherlands (Dehnert et al., 2011). The denudation rate (E) prior distribution was translated into a mean of 30 m/Myr and standard
214 deviation of 24 m/Myr, with upper and lower bounds of 60 m/Myr and 0 m/Myr, respectively. The maximum value is based on geomorphological evidence presented in Fig. 4b, using the altitude difference between the Campine Plateau and the
216 adjacent Kleine Nete floodplain, and taking into account the youngest possible age for the Rhine sediments. The minimum value is set to equal the null-hypothesis, to encompass the scenario of the Campine Plateau being a residual relief due to
218 erosion-resistance of the substrate. The mean prior bulk density of the studied fluvial sediments was set to 1.65 g/cm^3, which is consistent with the average value of upper Neogene and Quaternary sediments in the region (Beerten et al., 2010). The full
220 range of the prior for bulk density was set between 1.5-1.8 g/cm^3, to allow for some variation in grain size, sorting and sediment packing. Bulk densities below 1.5 g/cm^3 are typical for clay-rich and or organic-rich soils, while densities in excess

Earth Surf. Dynam. Discuss., doi:10.5194/esurf-2016-57, 2016
Manuscript under review for journal Earth Surf. Dynam.
Published: 1 December 2016

of 1.8 g/cm^3 are typical for gravel-bearing sediments. However, none of these lithologies have been observed in such quantities so as to justify a wider prior range for the bulk density.

In contrast to the other model parameters, the prior distribution for the inherited ^{10}Be concentration, N_{inh}, was assumed to be uniform. This is because solutions for N(z,t) in Eq. (1) always converge to N_{inh} as z tends to infinity while no N_{inh} measurements are available at z larger than 3.5 m. The N_{inh} parameter was therefore allowed to vary uniformly between two extreme values. The maximum value of 9×10^4 at/g is consistent with the highest concentration measured in the profile (Table 2; the inherited concentration cannot be higher than this value). The lower bound was somewhat arbitrarily set at 1×10^4 at/g, given the fact that zero inheritance is considered to be very unlikely.

Lastly, a so-called Jeffreys (1946) prior of the form $p(\sigma) \propto 1/\sigma$ is used for σ. This classical choice basically means that one wants to achieve σ values that are both as small as possible and consistent with the data misfit.

3.3.3 Predictive uncertainty intervals

A 95 % uncertainty interval for the simulated CRN concentrations can be calculated by drawing parameter sets, $[\mathbf{x}, \sigma]$, from $p(\mathbf{x}|\mathbf{d})$ and removing the 2.5% largest and lowest values from the associated set of $F(\mathbf{x})$ responses. We call the so-derived 95 % uncertainty interval a "95 % uncertainty interval due to parameter uncertainty". Because of model inadequacy (that is, model errors), this interval may not bracket 95% of the observations though. Consistently with the assumptions underlying Eq. (5), we thus compute a "95% total uncertainty interval" by adding to each $F(\mathbf{x})$ a random noise $\mathbf{e} \propto N(0, \delta)$, with $\delta = \sigma - \sigma_m$ where σ_m is a fixed measurement error which we take as the maximum analytic measurement error of our dataset, that is, $\sigma_m = 2000$ atoms/g.

4 Results

4.1 CRN profiling technique

Table 2 lists sample input parameters, and measured ^{10}Be concentrations with analytical errors. The depth is given below the contact with the overlying aeolian sand cover. In general, there is a clear decrease in ^{10}Be concentration with depth, except for two samples (-04 and -06) which clearly contain higher CRN concentrations (Fig. 6). It is striking that the CRN concentrations are consistently higher for the two samples were the finer (250-500 µm) grain size fraction was analysed. Grain size-dependent ^{10}Be concentrations can point to differences in geomorphological process rates in the regions of sediment provenance as suggested by Carretier et al. (2015). Alternatively, the negative relation between in-situ produced CRN and grain size might also result from non-stationary sedimentation rates, where samples from the fine-grained layers accumulated CRN during the final stage of the sedimentation cycle prior to a phase of non-deposition and/or steady state. Apart from the -04 and -06 samples , the CRN concentrations decrease non-linearly with depth, from $(1.5 \pm 0.02) \times 10^5$ at/g

Earth Surf. Dynam. Discuss., doi:10.5194/esurf-2016-57, 2016
Manuscript under review for journal Earth Surf. Dynam.
Published: 1 December 2016

252 at 10 cm to (9.0 ± 0.2) × 10^4 at/g at 320 cm. If we assume that the Campine Plateau is an erosion-resistant landform with negligibly low erosion rates ($E \approx 0$ cm/yr), the difference between $N_{total}(z)$ and N_{inh} gives the $N_{exp}(z)$ or the concentration of 254 cosmogenic nuclides that is produced at depth z after deposition of the Rhine sands. The apparent exposure age of the surface, t, can then be reconstructed following Eq. (1). By doing so, we obtain an apparent exposure age of 21.5 ± 1.5 ka, 256 which is in strong contradiction with chronostratigraphical age estimates of the fluvial deposits that cover the Campine Plateau that range between 0.5 and 1 Ma (see Section 2 and 3.3.2). We advocate that post-depositional erosion has strongly 258 altered the ^{10}Be signature of the upper layers of the Rhine sediments at the study site.

4.2 Posterior parameter distribution

260 The marginal posterior distributions of the 5 sampled parameters (including the standard deviation of the residual errors) are depicted in Fig. 7. The t distribution shows a weakly expressed mode around the prior mean value (Fig. 7a) whereas no 262 significant correlation is observed between t and the other model parameters except for N_{inh} with which a linear correlation of -0.13 is observed (Fig. 8a-d-f and Table 3). This means that the measurement data do not contain enough information to 264 resolve the exposure age. In other words, depending on the other model parameter values, the model can always fit the data no matter the value of t (within its prior range of 0.5 Ma - 1 Ma). The erosion rate, E, is much better resolved with a posterior 266 mode around 4.4 × 10^{-3} cm/yr which is equal to 44 mm/kyr or m/kyr (Fig. 7b). The posterior E uncertainty is relatively small, being 9 cm/yr (1σ) and 15 cm/yr (2σ). A large posterior linear correlation coefficient of 0.71 is found between E and 268 N_{inh} (Fig. 8c and Table 3). This suggests that one could try to fix one and only infer the other. The posterior bulk density distribution does not deviate much from its prior distribution (Fig. 7d), and shows a weak (negative) correlation with E (Fig. 270 8b and Table 3). The N_{inh} parameter shows a clear mode around 6.5 × 10^4 atoms/g, which is lower than the lowest measured value in the profile of about 9.09 × 10^4 atoms/g (Fig. 7d; Table 2). As mentioned already, a strong dependence with E was 272 found (Fig. 8c and Table 3). The standard deviation of the residual errors, σ, shows a log-normal marginal posterior with a clear mode around 1 × 10^4 atoms/g (Fig. 7e). This is consistent with the achieved root mean square error (RMSE) values 274 between measured and simulated ^{10}Be that follow a similar distribution with a mode about 1 × 10^4 atoms/g (not shown). It is interesting to note that with a range between 1.4 × 10^3 and 2 × 10^3 atoms/g, the analytical measurement errors are more than 276 5 times smaller than the values taken by σ. This nicely illustrates the effect of model errors. If the model would have been perfect, the achieved RMSE values and σ distribution should indeed have been within this measurement error range of 1.4 × 278 10^3 to 2 × 10^3 atoms/g.

Fig. 9 presents the 95 % predictive uncertainty interval due to parameter uncertainty (dark gray area) together with the 95 % 280 total predictive uncertainty interval (light gray area). Indeed, the 95 % uncertainty interval due to parameter uncertainty brackets only 6 observations out of 7, which is less that what would be expected from a 95 % confidence level. This gap is 282 likely caused by model inadequacy. The derived 95 % total predictive uncertainty interval is much larger and encapsulates all of the 7 observed data.

Earth Surf. Dynam. Discuss., doi:10.5194/esurf-2016-57, 2016
Manuscript under review for journal Earth Surf. Dynam.
Published: 1 December 2016

Earth Surface Dynamics Discussions Open Access EGU

5 Discussion

Five parameters of the CRN model were considered to be uncertain within the MCMC inversion: E, t, N_{inh}, ρ and σ. With only seven measurement data, the chosen marginal prior distributions for these parameters are obviously strongly influencing the sampled posterior distribution. Moreover, as stated earlier, we used relatively flat distributions with wide ranges such that the search towards the maximum a posteriori (MAP) prediction is not much constrained by the prior. This resulted in a poor resolution for the t and ρ parameters (Fig. 7a and 7c) for which marginal prior and posterior distributions are quite similar. In contrast, the inherited ^{10}Be concentration (N_{inh}) appears to be a well-resolved parameter. This is an important observation, because for eroding surfaces such as the one considered in this study, the inherited concentration contributes significantly to the total ^{10}Be concentration. The target parameter in this study, that is, the erosion rate (E), appears to be well-resolved as well, showing a relatively tight posterior distribution that is shifted towards higher mean values compared to the prior (Fig. 7b). In the following, the posterior mean of the E distribution, together with a one sigma uncertainty level, i.e. 44 ± 9 m/Myr or mm/kyr, are used to discuss the inferred erosion rate.

In Fig. 10, the pooled erosion rate data for outcrops, as published by Portenga and Bierman (2011) are shown, together with the mean erosion rate obtained in the present study. The global erosion data are based on surface samples (thickness ranging between 0.5 cm and 8 cm) from a variety of bedrocks, including igneous, metamorphic and sedimentary rocks, and various climato-tectonic settings. Generally speaking, outcrop erosion rates from Portenga and Bierman (2011) tend to be lower than the one determined for the headwaters of the Nete catchment, with a few exceptions. Since their data set is entirely based on bedrock samples, we argue that the differences in erosion rate principally reflect differences in erosion resistance of the substrate, i.e., consolidated rock versus unconsolidated sediment. Furthermore, in a western European context, the erosion rate that we report here seems to be fairly high for a fluvial terrace. For comparison, the Meuse younger Main Terrace (YMT) near Liège does not show any signs of post-depositional erosion following Rixhon et al. (2011). Probably, the coarse-grained and slightly consolidated nature of the Meuse sediment can be put forward as an explanation. Similarly, Dehnert et al. (2011) reported that the High Terraces of the Rhine in Germany and the Netherlands were eroded by only 1-3 m, and that the loess cover presumably protected the Rhine sands from significant erosion soon after deposition.

An alternative explanation for the relatively high erosion rate found in the current study may be the proximity of the North Sea, and its changes in base level during sea level lowstands. In contrast to the Meuse and Rhine, the Scheldt basin, to which the studied Rhine terrace belongs today, developed in response to the sudden base level lowering as a result of the opening of the English Channel, ca. 450 ka ago (see Section 2). An important feature of the Scheldt basin is the Flemish Valley, a buried river system, which the Nete basin is an eastern extension from. We advocate that the sudden base level lowering may have caused a regressive erosion wave penetrating into the hinterland, shaping the Flemish Valley and its eastern extension, i.e. the Nete catchment, and cause increased erosion rates in this distal part of the Scheldt basin.

An important issue to tackle is to which extent the currently obtained erosion rate can be used to infer the total amount of erosion at the site. Mathematically, this translates into $E \times t$, and would roughly yield a value of between ca. 22 m (for t =

Earth Surf. Dynam. Discuss., doi:10.5194/esurf-2016-57, 2016
Manuscript under review for journal Earth Surf. Dynam.
Published: 1 December 2016

500 kyr) and 44 m (for t = 1 Myr). Adding up with the current thickness of fluvial sediment at the site (i.e., 5-10 m) this would mean that the original thickness of Rhine sediment would have been between ca. 27-54 m. Since this would exceed the thickness of Rhine sediment in the southwestern part of the Roer Valley Graben (Beerten, 2006), we consider this hypothesis to be false. Instead, we suggest that erosion started later, presumably after opening of the English Channel around 450 ka. The ^{10}Be data thus would reflect the arrival of the headward erosion wave in the distal part of the Nete catchment, following the opening of the English Channel, and the reorganisation of the hydrographical network. On the one hand this implies that the total amount of erosion is less than 22 m, according to the formula $E \times t$. On the other hand, at least 5-10 metres of extra sediment would have been needed to completely shield the sampled sediment from cosmogenic radionuclide production before the start of erosion, sometime after 450 ka.

In any case, there are several implications for the regional evolution of the landscape attached to the observation of sediment removal on top of the Campine Plateau. Firstly, it would mean that the total amount of Rhine sediment would have been larger than what can be observed today in the quarries (Fig. 4); this should be taken into account when correlating Rhine sediment from the Campine Plateau with that in the Roer Valley Graben. Secondly, post-depositional fault movement along (segments of) the Feldbiss fault as derived from the stratigraphy of Rhine sands should be considered as a minimum (Fig. 3). Thirdly, the amount of post-depositional erosion west of the plateau (Fig. 2) as can be observed from present-day altitude differences (Campine Plateau vs. Nete valley; Fig. 4b) should be regarded as a minimum erosion value.

In future work, the aim is to consider more parameters in the MCMC inversion when new and more densely sampled profiles become available. Moreover, in an attempt to account for differences in geomorphological process rates in the regions of sediment provenance or non-stationary sedimentation rates, resulting in grain-size dependent ^{10}Be concentrations, the MCMC simulation could be combined with a distributed numerical forward modelling approach instead of the currently used analytical solution.

6 Conclusion

In accordance with previous studies, we conclude and confirm that a single ^{10}Be concentration depth profile can generate meaningful and reliable information on the denudation rates of a given landform, even when several parameters are highly uncertain. An MCMC inverse modeling procedure leads to a maximum a posteriori post-depositional erosion rate of ca. 44 ± 9 m/Myr (mm/kyr) for the studied fluvial terrace of the Rhine which today belongs to the Nete catchment. This derived value of post-depositional erosion rate is fairly high compared to published outcrop erosion rate data in the Meuse and Rhine catchment, and elsewhere in the world. It is inferred that the unconsolidated nature of the studied sediment, the absence of a protecting cover (such as loess) and possibly also headward erosion in response to sudden base level lowering around 450 ka are put forward as a possible explanation. We conclude that MCMC modelling of ^{10}Be concentration depth profiles is a powerful tool to determine rates of landscape evolution and earth surface processes and to assess the associated uncertainties.

Earth Surf. Dynam. Discuss., doi:10.5194/esurf-2016-57, 2016
Manuscript under review for journal Earth Surf. Dynam.
Published: 1 December 2016

350

7 Code availability

352 A MATLAB code of the Bayesian inversion used in this study is available upon request to the second author.

8 Author contributions

354 K. Beerten designed the study, performed the sampling and prepared the manuscript with contributions from the second and third authors. E. Laloy implemented the model and performed the simulations. V. Vanacker prepared the samples, 356 interpreted and processed the raw data and performed initial calculations. B. Rogiers co-designed the study and L. Wouters supervised it.

358 9 Acknowledgements

This work is performed in close cooperation with, and with the financial support of NIRAS/ONDRAF, the Belgian Agency 360 for Radioactive Waste and Fissile Materials, as part of the programme on geological disposal of high-level/long-lived radioactive waste that is carried out by ONDRAF/NIRAS.

362

10 References

364 Balco, G., Stone, J.O., Lifton, N.A., Dunai, T.J.: A complete and easily accessible means of calculating surface exposure ages or erosion rates from 10Be and 26Al measurements, Quaternary Geochronology, 3, 174-195, 2008.

366 Beerten, K.: Toelichting bij de Quartairgeologische kaart, kaartblad (10-18) Beverbeek-Maaseik, Vlaamse Overheid, Departement Leefmilieu, Natuur en Energie, Brussel, 2005.

368 Beerten, K., Wemaere, I., Gedeon, M., Labat, S., Rogiers, B., Mallants, D., Salah, S., Leterme, B.: Geological, hydrogeological and hydrological data for the Dessel disposal site. Project near surface disposal of category A waste at 370 Dessel, NIROND–TR 2009–05 E V1, ONDRAF/NIRAS, Brussels, 2010.

Beerten, K., Dreesen, R., Janssen, J., Van Uytven, D.: The Campine Plateau, in: Demoulin, A. (Ed.): Geomorphology of 372 Belgium and Luxembourg, Springer Verlag, Berlin, in press.

Bogaart, P.W., van Balen, R.T.: Numerical modeling of the response of alluvial rivers to Quaternary climate change, Global 374 and Planetary Change, 27, 147-163, 2000.

Braucher, R., Brown, R.T., Bourles, D.L., Colin, F.: In-situ produced 10Be measurements at great depths: implicatins for production rates by fast muons, Earth and Planetary Science Letters, 221, 251-258, 2003.

Braucher, R., Del Castillo, P., Siame, L., Hidy, A.J., Bourlés, D.L.: Determination of both exposure time and denudation rate from an in situ-produced ^{10}Be depth profile: A mathematical proof of uniqueness. Model sensitivity and applications to natural cases, Quaternary Geochronology, 4, 56-67, 2009.

Carretier, S., Regard, V., Vassallo, R., Aguilar, G., Martinod, J., Riquelme, R., Christophoul, F., Charrier, R., Gayer, E., Farias, M., Audin, L., Lagane, C.: Differences in 10Be concentrations between river sand, gravel and pebbles along the western side of the central Andes, Quaternary Geochronology, 27, 33-51, 2015.

Campforts, B., Vanacker, V., Vanderborght, J., Baken, S., Smolders, E., Govers, G.: Simulating the mobility of meteoric ^{10}Be in the landscape through a coupled soil-hillslope model (Be2D), Earth and Planetary Science Letters, 439, 143-157, 2016.

Chmeleff, J., von Blanckenburg, F., Kossert, K., Jakob, D.: Determination of the 10Be half-life by multicollector ICP-MS and liquid scintillation counting, Nuclear Instruments and Methods in Physics Research B, 263, 192-199, 2010.

Cloething, S.A.P.L., Ziegler, P.A., Bogaard, P.J.F., 30 co-workers and TOPO-EUROPE Working Group: TOPO-EUROPE: The geoscience of coupled deep Earth-surface processes, Global and Planetary Change, 58, 1-118, 2007.

Deckers, J., Vernes, R.W., Dabekaussen, W., Den Dulk, M., Doornenbal, J.C., Dusar, M., Hummelman, H.J., Matthijs, J., Menkovic, A., Reindersma, R.N., Walstra, J., Westerhoff, W.E., Witmans, N.: Geologisch en hydrogeologisch 3D model van het Cenozoïcum van de Roerdalslenk in Zuidoost-Nederland en Vlaanderen (H3O-Roerdalslenk). Studie uitgevoerd door VITO, TNO-Geologische Dienst Nederland en de Belgische Geologische Dienst in opdracht van de Afdeling Land en Bodembescherming, Ondergrond, Natuurlijke Rijkdommen van de Vlaamse overheid, de Afdeling Operationeel Waterbeheer van de Vlaamse Milieumaatschappij, de Nederlandse Provincie Limburg en de Nederlandse Provincie Noord-Brabant, VITO en TNO-Geologische Dienst Nederland, 2014

Dehnert, A., Kracht, O., Preusser, F., Akçar, N., Kemna, H.A., Kubik, P.W., Schlüchter, C.: Cosmogenic isotope burial dating of fluvial sediments from the Lower Rhine Embayment, Germany, Quaternary Geochronology, 6, 313-325, 2011.

Foster, M.A., Anderson, R.S., Wyshnytzky, C.E., Ouimet, W.B., Dethier, D.P.: Hillslope lowering rates and mobile-regolith residence times from in situ and meteoric 10Be analysis, Boulder Creek Critical Zone Observatory, Colorado, Geological Society of America Bulletin, 127, 862-878, 2015.

Gibbard, P.L.: Europe cut adrift, Nature, 448, 259-260, 2007.

Gosse, J.C., Philips, F.M.: Terrestrial in-situ cosmogenic nuclides: theory and application, Quaternary Science Reviews 20, 1475-1560, 2001.

Gullentops, F., Bogemans, F., De Moor, G., Paulissen, E., Pissart, A.: Quaternary lithostratigraphic units (Belgium), Geologica Belgica, 4, 153-164, 2001.

Gupta, S., Collier, J.S., Palmer-Felgate, A., Potter, G.: Catastrophic flooding origin of shelf valley systems in the English Channel, Nature, 448, 342–345, 2007.

Hancock, G.S., Anderson, B.S., Chadwick, O.A., Finkel, R.C.: Dating fluvial terraces with 10Be and 26Al profiles: Application to the Wind River, Wyoming, Geomorphology, 27, 41-60, 2009.

Kubik, P.W., Christl, M.: 10Be and 26Al measurements at the Zurich 6 MV Tandem AMS facility, Nuclear Instruments and Methods in Physics Research B, 268, 880-883, 2010.

Jeffreys, H.: An invariant form for the prior probability in estimation problems, Proc. R. Soc. London, Ser. A, 186, 453-461, 1946.

Laloy, E., Vrugt, J. A.: High-dimensional posterior exploration of hydrologic models using multiple-try DREAM(ZS) and high-performance computing, Water Resour. Res., 48, W01526, 1-18, 2013.

Miller, K.G., Kominz, M.A., Browning, J.V., Wright, J.D., Mountain, G.S., Katz, M.E., Sugarman, P.J., Cramer, B.S., Christie-Blick, N., Pekar, S.F.: The Phanerozoic record of global sea-level change, Science, 310, 1293-1298, 2005.

Norton, K.P., Vanacker, V.: Effects of terrain smoothing on topographic shielding correction factors for cosmogenic nuclide-derived estimates of basin-averaged denudation rates, Earth Surface Processes and Landforms, 34, 146-154, 2009.

Paulissen, E.: De Morfologie en de Kwartairstratigrafie van de Maasvallei in Belgisch Limburg, Verh. Kon. Acad. Wetensch., Letteren en Schone Kunsten v. België, Kl. der Wetensch., 127, 1-266, 1973.

Paulissen, E.: Les nappes alluviales et les failles Quaternaires du Plateau de Campine, in: Robaszynski, F., Dupuis, C. (Eds.): Guides Géologiques Régionaux – Belgique, Masson, Paris, 167-170, 1983.

Portenga, E.W., Bierman, P.R.: Understanding Earth's eroding surface with 10Be, GSA Today, 21, 4-10, 2011.

Rixhon, G., Braucher, R., Bourlès, D., Siame, L., Bovy, B., Demoulin, A.: Quaternary river incision in NE Ardennes (Belgium) – Insights from 10Be/26Al dating of river terraces, Quaternary Geochronology, 6, 273-284, 2011.

Robert, C., Casella, G.: Monte Carlo statistical methods, Springer texts in statistics, Springer, 580 pp., 2004.

Schaller, M., von Blanckenburg, F., Hovius, N., Kubik, P.W.: Large-scale erosion rates from in situ-produced cosmogenic nuclides in European river sediments, Earth and Planetary Science Letters, 188, 441-458, 2001.

Schokker, J., Cleveringa, P., Murray, A.S., Wallinga, J., Westerhoff WE, 2005. An OSL dated Middle and Late Quaternary sedimentary record in the Roer Valley Graben (southeastern Netherlands). Quaternary Science Reviews 24, 2243-2264

Siame, L., Bellier, O., Braucher, R., Sebrier, M., Cushing, M., Bourlès, D., Hamelin, B., Baroux, E., de Voogd, B., Raisbeck, G., Yiou, F.: Local erosion rates versus active tectonics: cosmic ray exposure modelling in Provence (south-east France), Earth and Planetary Science Letters, 220, 345-364, 2004.

Tavernier, R., De Moor, G.: L'évolution du Bassin de l'Escaut, in: Macar, P., Gullentops, F., Pissart, A., Tavernier, R., Zonneveld, J.I.S. (Eds.): L'évolution Quaternaire des bassins fluviaux de la mer du nord méridionale, Centenaire Soc. Géol. Belgique, p. 159-233, Liège, 1974.

ter Braak, C., Vrugt, J.: Differential Evolution Markov Chain with snooker updater and fewer chains, Stat. Comput. 18, 435–446, 2008.

van Balen, R.T., Houtgast, R.F., Van der Wateren, F.M., Vandenberghe, J., Bogaart, P.W.: Sediment budget and tectonic evolution of the Meuse catchment in the Ardennes and the Roer Valley Rift System, Global and Planetary Change, 27, 113-127, 2001.

Van Geet, M., De Craen, M., Beerten, K., Leterme, B., Mallants, D., Wouters, L., Cool, W., Brassinnes, S.: Climate evolution in the long-term safety assessment of surface and geological disposal facilities for radioactive waste in Belgium, Geologica Belgica, 15, 8-15, 2012.

Vanacker, V., von Blanckenburg, F., Govers, G., Molina, A., Poesen, J., Deckers, J., Kubik, P.: Restoring natural vegetation reverts mountain erosion to natural levels, Geology, 35, 303-306, 2007a.

Vanacker, V., von Blanckenburg, F., Hewawasam, T., Kubik, P.W.: Constraining landscape development of the Sri Lankan escarpment with cosmogenic nuclides in river sediment, Earth and Planetary Science Letters, 253, 402-414, 2007b.

Vandenberghe N., Van Simaeys S., Steurbaut E., Jagt J.W.M., Felder P.J.: Stratigraphic architecture of the Upper Cretaceous and Cenozoic along the southern border of the North Sea Basin in Belgium, Netherlands Journal of Geosciences, 83, 155-171, 2004.

Vandenberghe, J., De Smedt, P.: Palaeomorphology in the eastern Scheldt basin (Central Belgium) - The dijle-demer-grote nete confluence area, Catena, 6, 73-105, 1979.

von Blanckenburg, F.: The control mechanisms of erosion and weathering at basin scale from cosmogenic nuclides in river sediment, Earth Planetary Science Letters, 237, 462-479, 2005.

von Blanckenburg, F., Belshaw, N. S., O'Nions, R. K.: Separation of ^{9}Be and cosmogenic ^{10}Be from environmental materials and SIMS isotope dilution analysis, Chemical Geology, 129, 93-99, 1996.

Vrugt, J. A., Braak, C. J. F. T., Diks, C. G. H., Robinson, B. A., Hyman, J. M., Higdon, D.: Accelerating Markov chain Monte Carlo simulation by differential evolution with self-adaptive randomized subspace sampling, Int. J. Nonlin. Sci. Num., 10, 273–290, 2009.

Westaway, R.: Flow in the lower continental crust as a mechanism for the Quaternary uplift of the Rhenish Massif, north-west Europe, in: Maddy, D., Macklin, M.G., Woodward, J.C. (Eds.): River basin sediment systems: archives of environmental change, Balkema, Lisse, p. 87-167, 2001.

Westerhoff, W.E., Kemna, H.A., Boenigk, W.: The confluence area of Rhine, Meuse, and Belgian rivers: Late Pliocene and Early Pleistocene fluvial history of the northern Lower Rhine Embayment, Netherlands Journal of Geosciences, 87, 107-125, 2008.

Earth Surf. Dynam. Discuss., doi:10.5194/esurf-2016-57, 2016
Manuscript under review for journal Earth Surf. Dynam.
Published: 1 December 2016

476 Figure Captions

478 Figure 1 – Location of the Campine region within Europe and the European Sand Belt.

480 Figure 2 – Structural map of northwestern Europe showing the Roer Valley Graben faults and the Brabant and Rhenohercynian (Ardennes) massifs superimposed on a Digital Terrain Model (DTM) of northwestern Europe (GTOPO30; 482 data available from the U.S. Geological Survey), with indication of large rivers (http://www.eea.europa.eu/data-and-maps/data/wise-large-rivers-and-large-lakes) and location of the Scheldt basin, (dashed line), the Nete catchment (dotted 484 line) and the Flemish Valley (solid line). The general palaeohydrography of the Meuse and Rhine between 0.5 Ma and 1.0 Ma is shown in coloured lines. Headward erosion as an explanation for the development of the Nete catchment is indicated 486 with a yellow arrow.

488 Figure 3 – DTM of the Campine Plateau (Digitaal Hoogtemodel Vlaanderen II, DTM, raster, 1 m) and the extent of Rhine deposits in the study area (shading; based on Beerten (2005) and Deckers et al. (2014)).

490

Figure 4 – (a): Detailed DTM of the study area (Digitaal Hoogtemodel Vlaanderen II, DTM, raster, 1 m), with indication of 492 the sampling location (white arrow). Note the regularly shaped sand quarries south of profile line A-A' which appear as depressions on the DTM. (b): Topographic cross-section according to the profile line (A-A') shown in (a). The sampling 494 location is schematically shown as a grey rectangle.

496 Figure 5 – Photograph of the sampled profile with indication of sampling points, field codes, lithological units (A-G) and approximate profile depth.

498

Figure 6 – ^{10}Be concentration profile and results of the grain size analyses. Note that the elevated ^{10}Be concentrations belong 500 to samples that were analysed using a smaller grain size fraction than the other samples (i.e., 250-500 µm instead of 500-1000 µm).

502

Figure 7 – Posterior distributions of the six parameters. (a): exposure age. (b): erosion rate. (c): bulk density. (d): inherited 504 ^{10}Be concentration. (e): standard deviation of the residual errors.

506 Figure 8 – Selected correlation plots for the five parameters. Note that N_{inh} and E show the strongest correlation.

Earth Surf. Dynam. Discuss., doi:10.5194/esurf-2016-57, 2016
Manuscript under review for journal Earth Surf. Dynam.
Published: 1 December 2016

508 Figure 9 – 95 % predictive uncertainty interval due to parameter uncertainty and the 95 % total predictive uncertainty interval (dark gray area). Depth is given in cm below the contact with the overlying aeolian sand cover.

510

Figure 10 – Frequency distribution of the pooled outcrop erosion rates obtained from Portenga and Bierman (2011), with
512 indication of the mean value obtained for the Nete catchment (this study).

Earth Surf. Dynam. Discuss., doi:10.5194/esurf-2016-57, 2016
Manuscript under review for journal Earth Surf. Dynam.
Published: 1 December 2016

Earth Surface Dynamics Discussions
Open Access
EGU

Table 1 - Prior distributions for four parameters: erosion rate, exposure age, bulk density and inherited ^{10}Be concentration.

Parameter	Symbol	Unit	Distribution	Min-max	Mean	St. dev.
Erosion rate	*E*	m/Myr or mm/kyr	Truncated Gaussian	0 – 60	30	24
Exposure age	*t*	Ma	Truncated Gaussian	0.5 – 1.0	0.75	0.2
Bulk density	ρ	g/cm^3	Truncated Gaussian	1.5 – 1.8	1.65	0.12
Inherited ^{10}Be	N_{inh}	10^4 atoms/g	Uniform	1 – 9	n/a	n/a

Table 2 - Analytical results from the in-situ produced 10Be analysis. The depth profile is located at 50.95°N and 5.63°W at an altitude of 47 m. A SLHL (sea-level high-altitude) production rate of 4.5 ± 0.3 at/g/y was used in this study. We refer to the text for more information on the methodology used.

Sample label	Sample field code	Relative depth z_{fluv} (cm)*	Quartz (g)	Be carrier (mg)	^{10}Be/^{9}Be (× 10^{-12})	^{10}Be conc (× 10^5at/g qtz)
TB1204	BE-MHR-II-00	10	34,406	0,208	0,388 ± 0,016	1,537 ± 0,019
TB1205	BE-MHR-II-01	40	33,535	0,207	0,329 ± 0,016	1,328 ± 0,017
TB1206	BE-MHR-II-02	60	33,370	0,207	0,252 ± 0,016	1,015 ± 0,015
TB1207	BE-MHR-II-03	80	34,467	0,207	0,318 ± 0,016	1,245 ± 0,017
TB1940	BE-MHR-II-04	120	23,478	0,164	0,521 ± 0,019	2,397 ± 0,029
TB1208	BE-MHR-II-05	160	34,620	0,207	0,231 ± 0,015	0,898 ± 0,014
TB1944	BE-MHR-II-06	200	23,486	0,164	0,709 ± 0,043	3,272 ± 0,037
TB1209	BE-MHR-II-07	240	34,186	0,207	0,251 ± 0,014	0,987 ± 0,015
TB1210	BE-MHR-II-09	320	33,663	0,207	0,229 ± 0,014	0,909 ± 0,015
TB1211	BE-BLANK-01	NA	0,000	0,207	0,0011 ± 0,0006	
TB1941	BE-BLANK-02	NA	0,000	0,164	0,0041 ± 0,0009	

**The relative depth z_{fluv} is given as depth below the contact with the overlying aeolian sand cover.*

Earth Surf. Dynam. Discuss., doi:10.5194/esurf-2016-57, 2016
Manuscript under review for journal Earth Surf. Dynam.
Published: 1 December 2016

Earth Surface Dynamics Discussions
Open Access
EGU

Table 3 – Posterior linear correlation coefficients between the 5 sampled variables.

Sampled parameter	E	t	ρ	N_{inh}	σ
E	1				
t	0.017	1			
ρ	-0.221	-0.002	1		
N_{inh}	0.709	-0.139	0.197	1	
σ	-0.110	0.007	-0.082	-0.145	1

Earth Surf. Dynam. Discuss., doi:10.5194/esurf-2016-57, 2016
Manuscript under review for journal Earth Surf. Dynam.
Published: 1 December 2016

Earth Surface Dynamics Discussions
Open Access
EGU

Figure 01

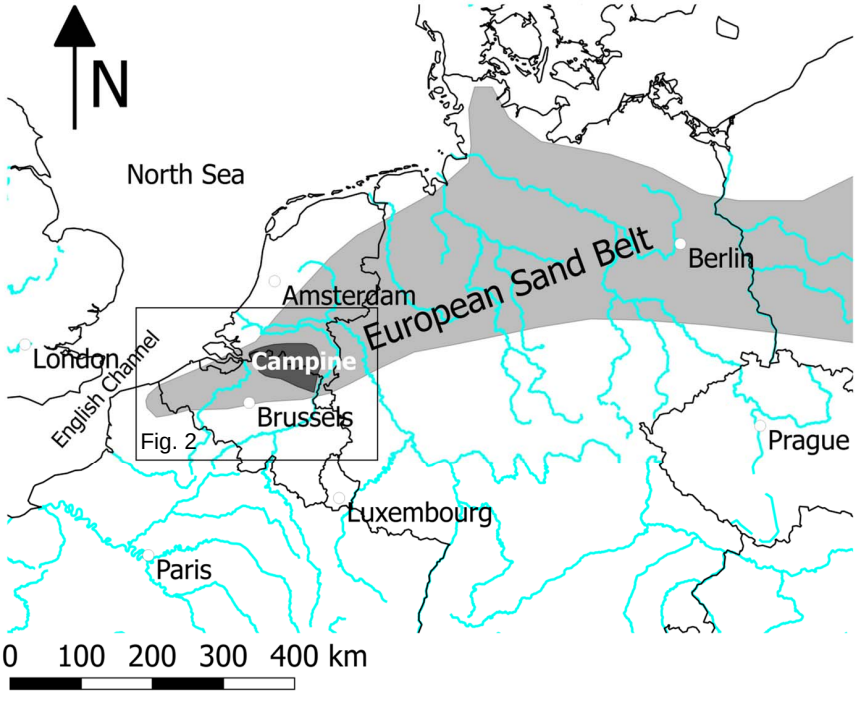

Earth Surf. Dynam. Discuss., doi:10.5194/esurf-2016-57, 2016
Manuscript under review for journal Earth Surf. Dynam.
Published: 1 December 2016

Earth Surface Dynamics Discussions
Open Access
EGU

Figure 02

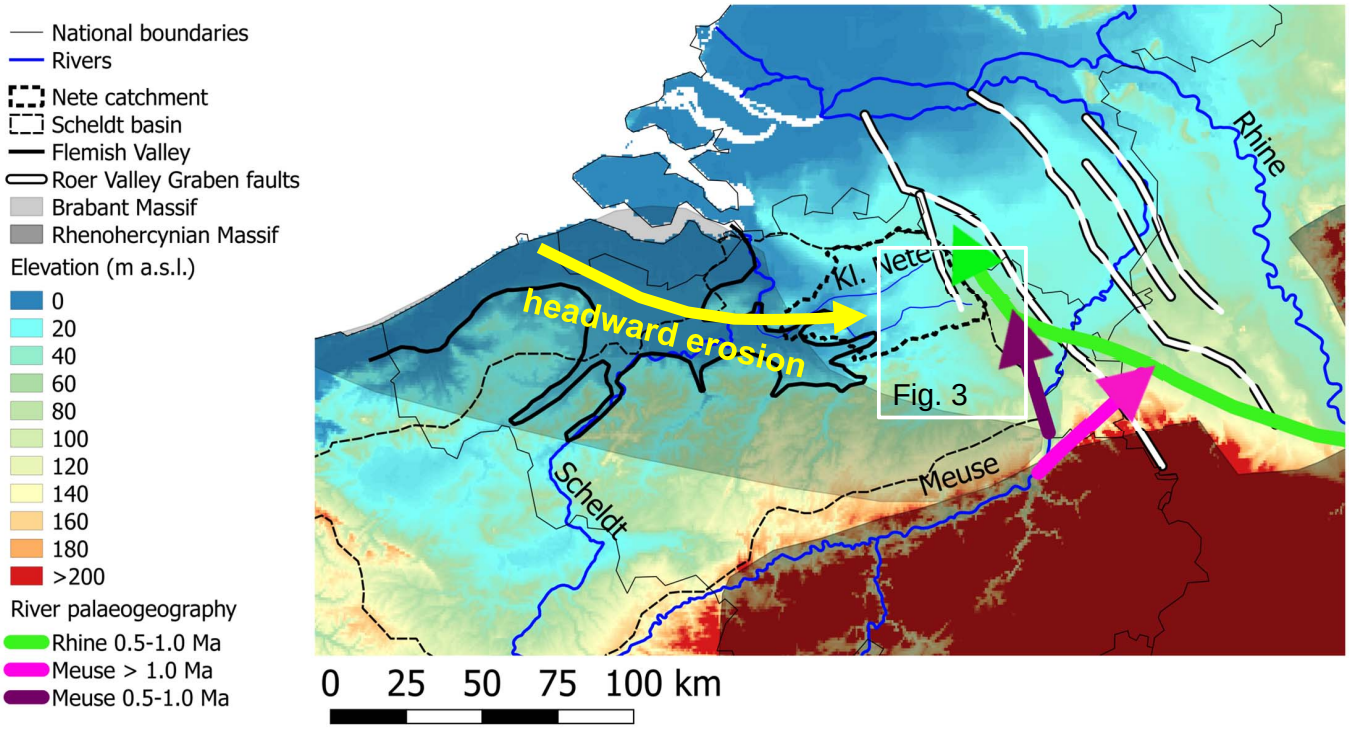

Earth Surf. Dynam. Discuss., doi:10.5194/esurf-2016-57, 2016
Manuscript under review for journal Earth Surf. Dynam.
Published: 1 December 2016

Earth Surface Dynamics Discussions
Open Access
EGU

Figure 03

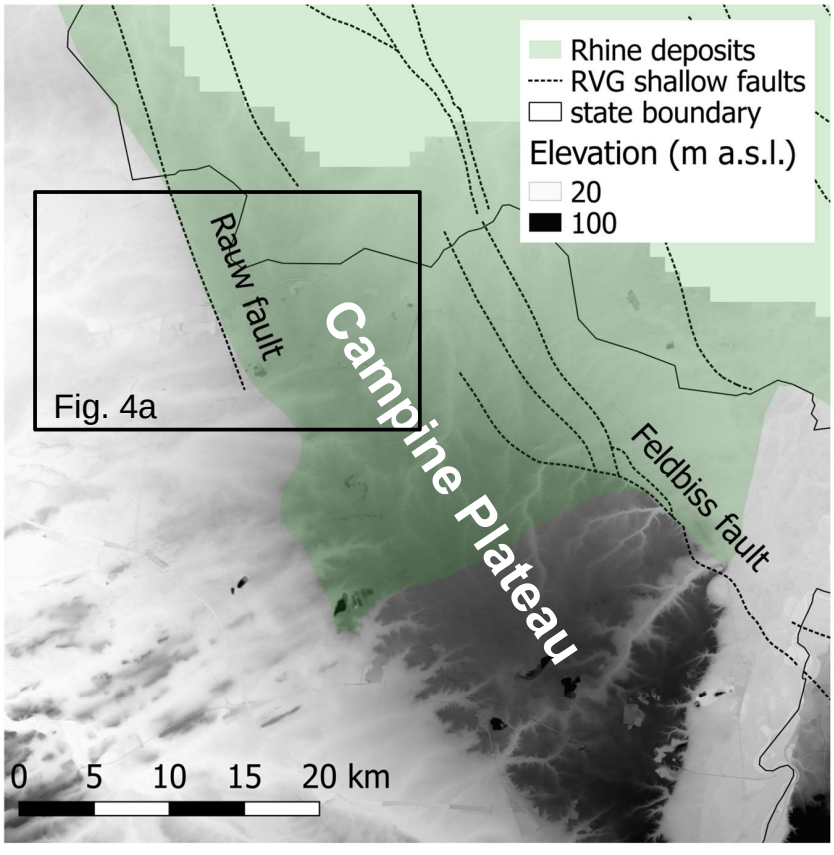

Earth Surf. Dynam. Discuss., doi:10.5194/esurf-2016-57, 2016
Manuscript under review for journal Earth Surf. Dynam.
Published: 1 December 2016

Figure 04

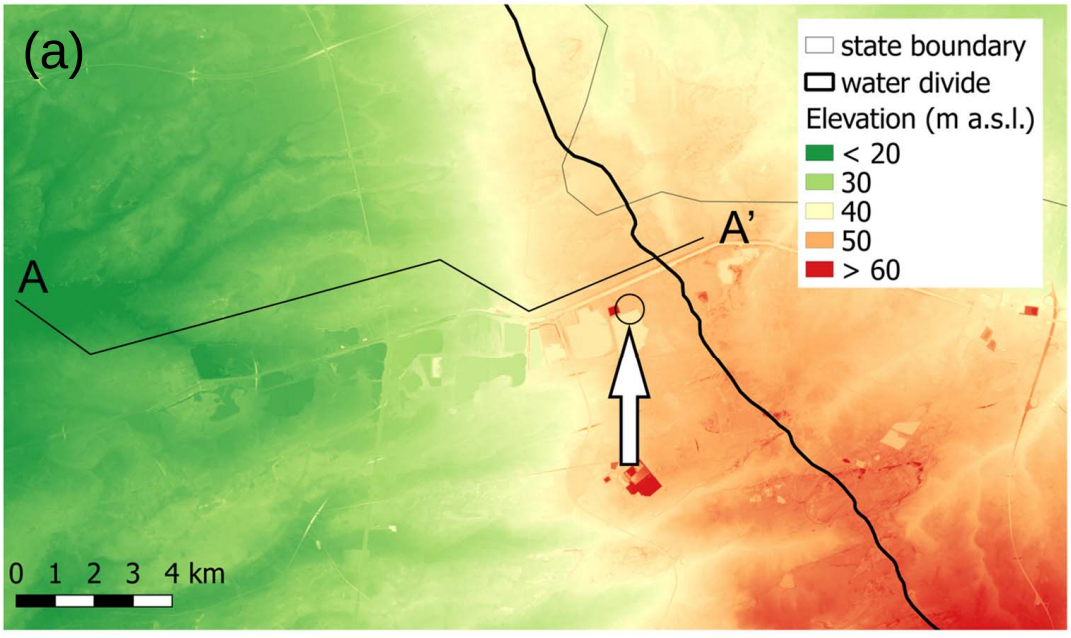

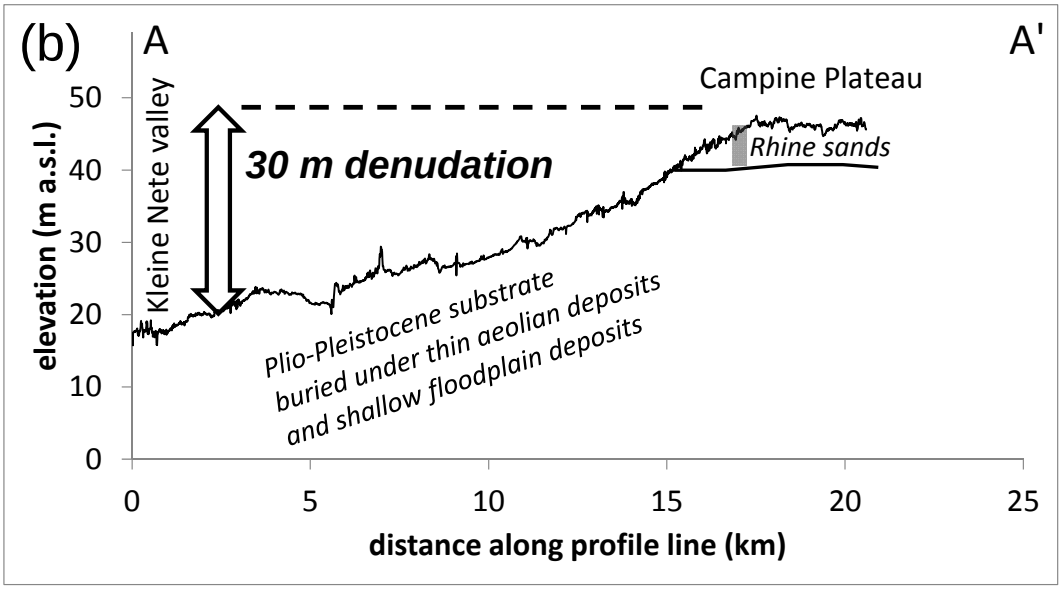

Earth Surf. Dynam. Discuss., doi:10.5194/esurf-2016-57, 2016
Manuscript under review for journal Earth Surf. Dynam.
Published: 1 December 2016

Earth Surface Dynamics Discussions
Open Access
EGU

Figure 05

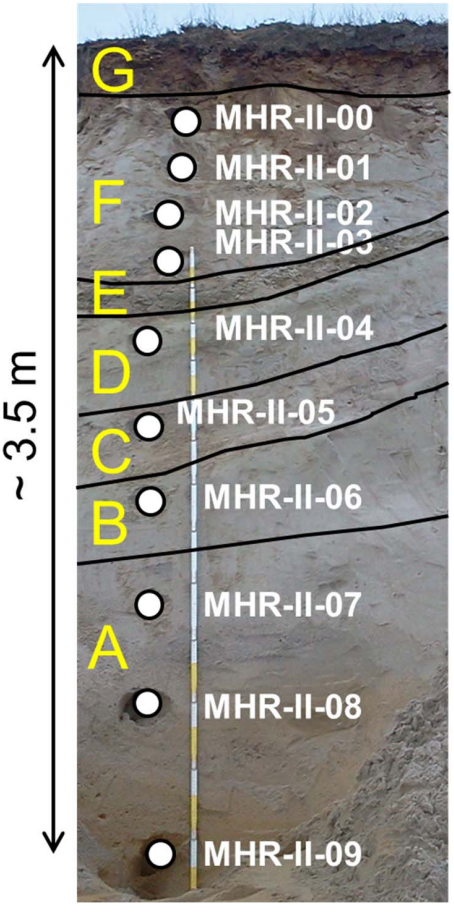

Earth Surf. Dynam. Discuss., doi:10.5194/esurf-2016-57, 2016
Manuscript under review for journal Earth Surf. Dynam.
Published: 1 December 2016

Figure 06

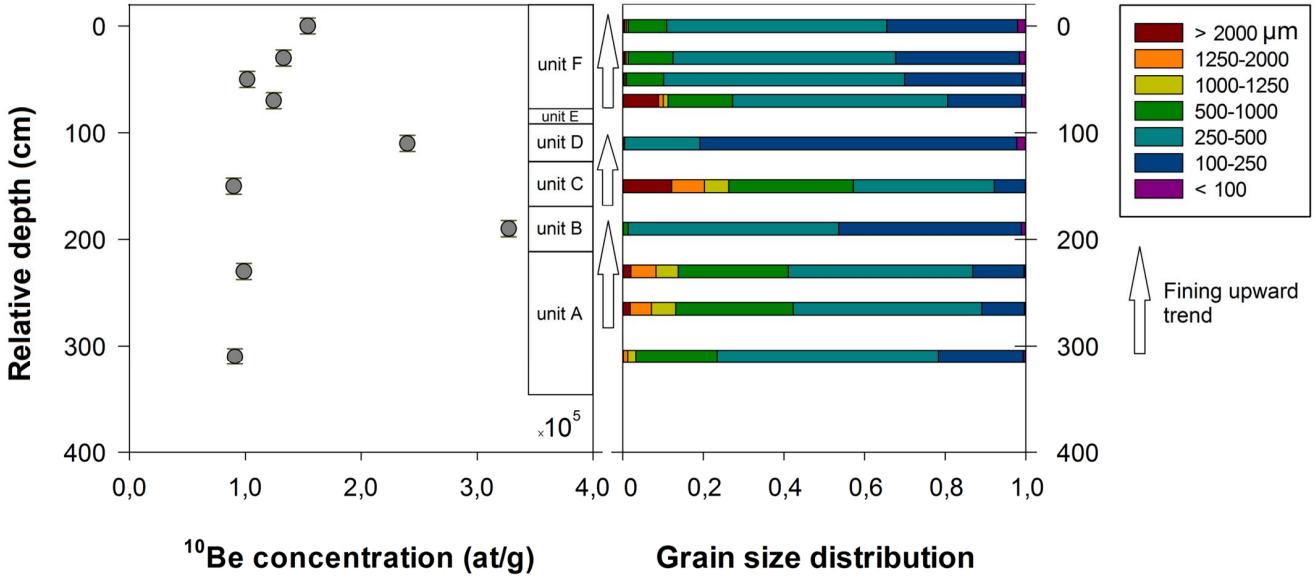

Earth Surf. Dynam. Discuss., doi:10.5194/esurf-2016-57, 2016
Manuscript under review for journal Earth Surf. Dynam.
Published: 1 December 2016

Figure 07

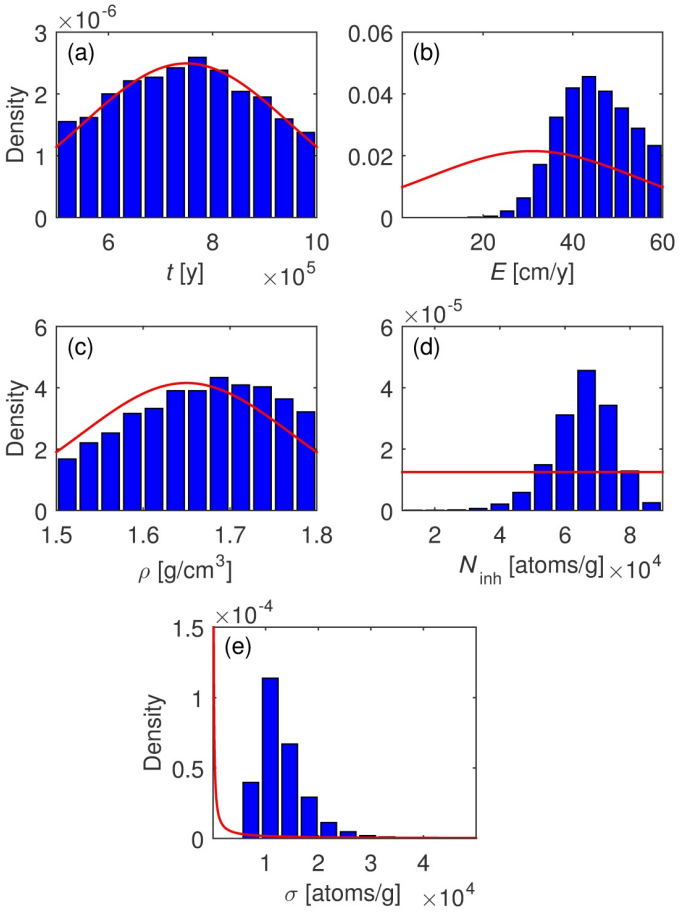

Earth Surf. Dynam. Discuss., doi:10.5194/esurf-2016-57, 2016
Manuscript under review for journal Earth Surf. Dynam.
Published: 1 December 2016

Earth Surface Dynamics Discussions
Open Access
EGU

Figure 08

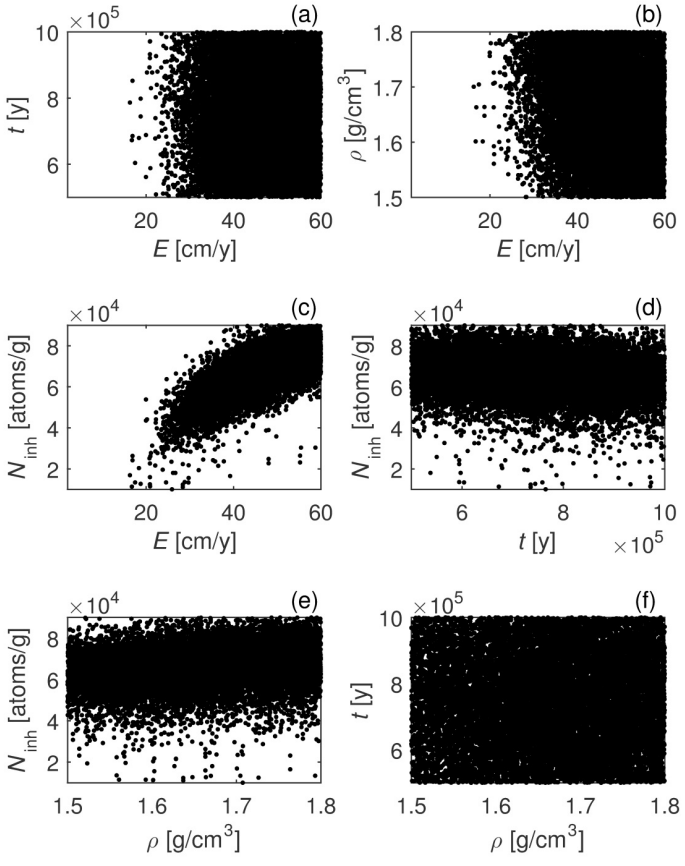

Earth Surf. Dynam. Discuss., doi:10.5194/esurf-2016-57, 2016
Manuscript under review for journal Earth Surf. Dynam.
Published: 1 December 2016

Earth Surface Dynamics Discussions
Open Access
EGU

Figure 09

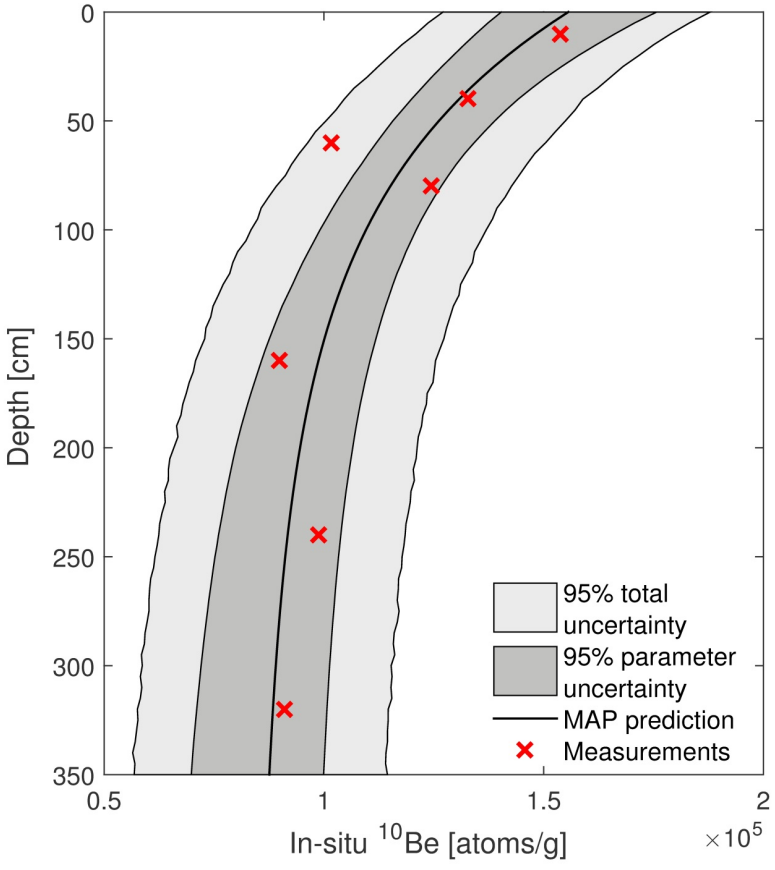

Earth Surf. Dynam. Discuss., doi:10.5194/esurf-2016-57, 2016
Manuscript under review for journal Earth Surf. Dynam.
Published: 1 December 2016

Earth Surface Dynamics Discussions
Open Access
EGU

Figure 10